Title

Detection of High-Risk Paraneoplastic Antibodies against TRIM9 and TRIM67 Proteins

Permalink

Journal

ISSN

Authors

Bartley, Christopher M
Ngo, Thomas T
Duy, Le
et al.

Publication Date

DOI

Peer reviewed

Detection of High-Risk Paraneoplastic Antibodies Against TRIM9 and TRIM67 proteins

Christopher M. Bartley, M.D., Ph.D.[1,2], **Thomas T. Ngo, B.S.**[1,2,6], **Le Duy Do, Ph.D.**[3], **Anastasia Zekeridou, M.D., PhD**[4,5], **Ravi Dandekar, B.S., M.S.**[1,6], **Sergio Muñiz-Castrillo, M.D., Ph.D.**[3], **Bonny D. Alvarenga, B.A.**[1,6], **Kelsey C. Zorn, B.A., M.H.S.**[10], **Asritha Tubati, B.S.**[1,6], **Anne-Laurie Pinto, M.Sc.**[3], **Weston D. Browne, B.S.**[1,6], **Patrick W. Hullett, M.D., Ph.D.**[1,6], **Mark Terrelonge, M.D., M.P.H.**[1,6], **Ryan D. Schubert, M.D.**[1,6], **Amanda L. Piquet, M.D.**[7], **Binxia Yang, Ph.D.**[5], **Mayra J. Montalvo Perero, M.D.**[4], **Andrew F. Kung, B.A.**[8], **Sabrina A. Mann, B.S.**[9,10], **Maulik P. Shah, M.D., M.H.S.**[1,6], **Michael D. Geschwind, M.D., Ph.D.**[1,6], **Jeffrey M. Gelfand, M.D., M.A.S.**[1,6], **Joseph L. DeRisi, Ph.D.**[9,10], **Sean J. Pittock, M.D.**[4,5], **Jérôme Honnorat, M.D., Ph.D.**[3], **Samuel J. Pleasure, M.D., Ph.D.**[†,1,6], **Michael R. Wilson, M.D., M.A.S.**[†,1,6]

[1]Weill Institute for Neurosciences, University of California, San Francisco, California

[2]Department of Psychiatry and Behavioral Sciences, University of California San Francisco, California

[3]French Reference Center on Paraneoplastic Neurological Syndromes and Autoimmune Encephalitis, Hospices Civils de Lyon and SynatAc Team, Institut MELiS, INSERM U1314/CNRS UMR 5284, Universités de Lyon, Université Claude Bernard Lyon 1, Lyon, France

[4]Department of Neurology, Center MS and Autoimmune Neurology, Mayo Clinic

[5]Department of Laboratory Medicine and Pathology, Mayo Clinic

[6]Department of Neurology, University of California, San Francisco, California

[7]Department of Neurology, University of Colorado Anschutz Medical Campus, School of Medicine, Aurora, Colorado

[8]University of California San Francisco, School of Medicine, San Francisco, California

[9]Chan Zuckerberg Biohub, San Francisco, California

¹⁰Department of Biochemistry and Biophysics, University of California, San Francisco, California

Abstract

Co-occurring anti-tripartite motif-containing protein 9 and 67 autoantibodies (TRIM9/67-IgG) have been reported in only a very few cases of paraneoplastic cerebellar syndrome. The value of these biomarkers and the most sensitive methods of TRIM9/67-IgG detection are not known. We performed a retrospective, multi-center study to evaluate the cerebrospinal fluid (CSF) and serum of candidate TRIM9/67-IgG cases by tissue-based immunofluorescence (TBIF), peptide phage display immunoprecipitation sequencing (PhIP-Seq), overexpression cell-based assay (CBA), and immunoblot. Cases in whom TRIM9/67-IgG was detected by at least two assays were considered TRIM9/67-IgG positive. Among these cases (N=13), CBA was the most sensitive (100%) and revealed that all cases had TRIM9 and TRIM67 autoantibodies. Of TRIM9/67-IgG cases with available clinical history, a subacute cerebellar syndrome was the most common presentation (N = 7/10), followed by encephalitis (N = 3/10). Of these ten, 70% had comorbid cancer (7/10), 85% of whom (N = 6/7) had confirmed metastatic disease. All evaluable cancer biopsies expressed TRIM9 protein (N = 5/5), whose expression was elevated in the cancerous regions of the tissue in 4 of 5 cases. TRIM9/67-IgG are rare but likely high-risk paraneoplastic biomarkers for which CBA appears to be the most sensitive diagnostic assay.

Keywords

Introduction

Co-occurring TRIM9/67 autoantibodies (TRIM9/67-IgG) are proposed paraneoplastic biomarkers that are associated with a subacute pan-cerebellar syndrome, typically in the setting of lung cancer.[1–3] Importantly, TRIM9/67-IgG has not been detected in the sera or cerebrospinal fluid (CSF) of small cell lung cancer (SCLC) patients without a paraneoplastic neurological syndrome (PNS), autoimmune encephalitis patients, or patients with noninflammatory neurodegenerative disorders.[1] Therefore, TRIM9/67-IgG is not a general marker of cancer or neural injury. However, because only very few cases have been reported, the best detection method for TRIM9/67-IgG is unknown, and its usefulness as a paraneoplastic biomarker has not been definitively established.

Here we evaluated biospecimens from candidate TRIM9/67-IgG identified across three institutions by rodent brain tissue-based assay, immunoblot, overexpression cell-based assay (CBA), and pan-human proteome phage display immunoprecipitation sequencing (PhIP-Seq)[3,4]. The thirteen cases that were positive for TRIM9/67 antibodies by at least two methods were considered TRIM9/67-IgG positive. We reviewed these patients' medical histories and characterized available tumors from five of the TRIM9/67-IgG cases.

Methods

Human Subjects

Written informed consent was obtained from subjects or a surrogate (UCSF IRB 13–12236). Additional subjects were enrolled through the Mayo Clinic Neuroimmunology Laboratory (IRB 08–007810) and the NeuroBioTec Biobank (Hospices Civils de Lyon BRC, France, AC-2013-1867, NFS96–900, GenePNS, 19–62, NCT-03963700).

Evaluation of specificity of anti-TRIM9 and anti-TRIM67 antibodies used for murine and human TBIF and IHC

Because TRIM67 is a paralog of TRIM9 that arose through genome duplication[5] there is a risk of commercial antibody cross-reactivity. Therefore, we evaluated the specificity of the anti-TRIM9 (MyBioSource, MBS9603565, 1:100)[6,7] and anti-TRIM67 (Proteintech, 24369-1-AP, 1:25) antibodies that were used for mouse brain and tumor IHC by TRIM9-FLAG and TRIM67-FLAG overexpression CBAs. Sigma-Aldrich F1804 was used at 1:1000 to detect FLAG.

While the anti-TRIM67 antibody was specific to TRIM67, anti-TRIM9 was immunoreactive to both TRIM9 and TRIM67 (data not shown). However, TRIM9 and TRIM67 exhibited different subcellular distributions in HEK293T cells and mouse brain and TRIM9 expression generally did not overlap with TRIM67 in brain tissue. Moreover, the immunostaining patterns for TRIM9 and TRIM67 mirrored cell type-specific gene expression patterns of TRIM9 and TRIM67 in the murine cerebellum[8].

Cell-based Assays

To validate TRIM9/67 autoantibodies in CSF and sera, HEK 293 cells were transfected with pCS2-*TRIM9* plasmid (encoding N-terminal myc-tagged human TRIM9) or pCS2-*Trim67* plasmid[9] (encoding murine N-terminal myc-tagged Trim67). Fixed and permeabilized cells were immunostained with patient CSF (1:10) or serum (1:100) and a commercial rabbit monoclonal anti-Myc antibody (C3956, Sigma), and counterstained with the appropriate fluorochrome-conjugated secondary antibodies at 1:1000 (Fisher Scientific antibodies #A21433 and #A11034). CBAs were blindly read by three independent raters using fluorescent microscope Nikon Ni-U (Nikon SAS, Champigny-sur-Marne, France).

For B-box 2 domain CBAs, HEK 293T cells were plated onto 10mm poly-d-lysine coated (50μg/mL) coverslips in 24-well plates. Cells were transfected overnight using Lipofectamine 3000 with either pCMV6-hTRIM9-Myc-DDK (Origene), pCS2-hTRIM67-C-FLAG (Lyon), or pcDNA3.1(+)-C-DYK plasmids encoding amino acids 217–256 of human TRIM9 or amino acids 303–361 of human TRIM67 (Genscript). Transfected cells were rinsed with ice cold 1X PBS the following day, then fixed with 4% PFA for 10 minutes. Fixed cells were rinsed with PBS several times, then blocked and permeabilized for 30 minutes with 5% lamb serum in PBS containing 0.5% Triton X-100.

To screen for B-box 2 immunoreactivity, transfected cells were stained with anti-FLAG antibody at 1:1000 and CSF at 1:10 in 5% blocking buffer overnight at 4°C. Cells were

rinsed with PBS four times, then stained with Alexa Fluor secondaries at a 1:1000 dilution in 5% blocking buffer. Nuclei were stained with DAPI at 1μg/mL in PBS for 5 minutes. Stained slides were then mounted onto microscope slides with Prolong Gold antifade.

Animal Subjects

Tissue from postnatal day 40 – 60-day mice was used for immunostaining, immunoprecipitations, and immunoblotting (Jackson Laboratory F1 cross of FVB (Cat. No. #001800) x C57BL/6J (Cat. No. #000664)). Slides for indirect immunofluorescence on mouse tissue (brain, gut, kidney) were acquired (Scimedx). Animal procedures complied with federal guidelines and the institutional policies of the UCSF Institutional Animal Care (AN183338–02B) or Use Committee and the French Ethical Committee of the Lyon 1 University (DR2013–47) in accordance with European Community Council directive 2010/63/EU.

Rodent Brain Tissue-based Immunofluorescence:

At UCSF, mouse tissue was prepared as previously described[10] and incubated overnight with or without anti-TRIM9 or anti-TRIM67 antibodies at 4°C prior to secondary immunostaining and imaging using a Zeiss Axio Scan Z.1 Slide Scanner and Nikon CSU-W1 spinning disk confocal microscope followed by image preparation ImageJ (Version 2.1.0/1.53c).

At Mayo, specimens were tested on murine tissue cryosections as previously described[11] at screening dilutions of 1:240 for serum (preabsorbed with liver powder) or 1:2 for CSF.

At Lyon, freshly prepared adult rat brains were prepared as previously described[1] (but using 12 μm-thick sections) prior to immunostaining with CSF (1:10) and imaging on a ZEISS Axio Scan.Z1.

Tumor histology, immunohistochemistry, and multiplex immunofluorescence (mIF)

H&E slides were prepared in Leica Autostainer XL; slides stained in hematoxylin (Thermo Scientific Shandon Instant Hematoxylin cat. 6765015) for 7 minutes and in eosin (Thermo Scientific Shandon Instant Eosin-Y Alcoholic cat. 531946) for 20 seconds.

mIF staining was performed on the Ventana BenchMark Ultra using Discovery reagents (Ventana Medical Systems) according to manufacturer's instructions, except as noted. Heat Induced Epitope Retrieval (HIER) was performed with the Cell Conditioning 1 (CC1) solution (cat. 950–124) for 32 min at 97°C. Primary antibodies used were TRIM 9 (1:100, MBS710195), TRIM 67 (1:25, 24369-1-AP), ER (SP1, Abcam, ab1660, 1:50), and pan-CK (1:100, KRT/1877R, ab234297). The primary antibodies were detected with Discovery Red 610 Kit (cat. 760–245), FAM Kit (cat. 760–243) and Cy5 Kit (cat. 760–238) respectively. Finally, slides were counterstained with DAPI (Akoya cat. FP1490).

PhIP-Seq protocol and analysis

PhIP-Seq uses patient IgG to immunoprecipitate T7 bacteriophage that display 49 amino acid (AA) human peptides on their viral capsid. PhIP-seq was performed as previously described using two rounds of enrichment.[4]

To evaluate for TRIM9 and TRIM67 enrichment at the whole protein level, for each sample individual scaled peptide read counts (reads per 100,000, "rpK") were summed for TRIM9 and TRIM67. The Z score of the summed rpK for each protein for each sample relative to healthy control samples was calculated. A Z score 3 was interpreted as significantly enriched.

Chemiluminescent Immunoblot

Whole adult rat brains were first dislocated. The tissue was then homogenized in lysis buffer containing 50 mM Tris-HCl pH 7.5, 150 mM NaCl, 1 mM EDTA, 1% NP-40, 0.5% deoxycholate, 0.1% SDS, orthovanadate, benzonase, phosphatase inhibitor, and protease inhibitor. The homogenate was incubated on ice for 30 min and sonicated. Cell debris was discarded by 20 min centrifugation at 16000 g and 4°C. Then, 10 μg of whole brain protein extract were used for Western blotting to screen for bands recognized by patient CSF (1:100).

Immunoprecipitation mass spectrometry (IP-MS)

IP-MS was performed previously described.[10] Analysis was limited to spectral counting using Scaffold version 4.

Results

Clinical phenotypes of TRIM9/67-IgG positive cases

Clinical history for TRIM9/67-IgG cases was available for 10 of 13 cases as summarized in the Supplementary Table 1 and Supplemental Case Histories.

Cerebellar Syndrome

Seven of ten (cases 1–6 and 10) presented with subacute cerebellar syndrome, three of which (cases 2–4) were previously published.[1,2] All cerebellar syndrome cases developed a pan-cerebellar syndrome over 3–4 weeks. Additional features were noted in case 1, who developed cerebellar affective syndrome, and in case 3, who developed dysexecutive symptoms and anterograde amnesia.

Six of the seven cerebellar syndrome patients had cancer: lung adenocarcinoma (N = 3), SCLC (N = 1), melanoma (N = 1), and breast cancer (N = 1). Four developed the cerebellar syndrome after their cancer diagnosis. Among them, two (cases 1 and 2), developed the cerebellar syndrome after their second and fourth cycle of immune checkpoint inhibitor therapy, respectively. In the remaining two cases, the malignancy was found during work-up for a PNS. All six cancer patients had metastatic disease at the time of their neurological presentation.

Acute phase CSF testing revealed a mild to moderate lymphocytic pleocytosis in all cerebellar syndrome cases (8 – 74 cells/μL, ref.   5 cells/μL), whereas total protein was normal or modestly elevated (elevated in N = 3, 58 – 98 mg/dL, ref.   50 mg/dL). All four cases with available results had an elevated IgG index, three of whom also had CSF-restricted oligoclonal bands (OCBs). Commercial anti-neural autoantibody testing was negative in all cases. Only one of the six cases treated with at least one immunomodulatory agent showed improvement in neurologic symptoms (Supplementary Table 1).

Encephalitis

Of the three remaining cases with available clinical history (cases 7–9), two (cases 7 and 8) presented with subacute limbic encephalitis (LE) and one with subacute possible autoimmune encephalitis according to diagnostic criteria (case 9).[12]

Two of three encephalitis patients (cases 7 and 8) had a mild lymphocytic pleocytosis (16 and 6 cells/μL, respectively), had an elevated IgG index (1.9 and 1.1, respectively), and greater than five CSF-restricted OCBs (case 9 was not tested for OCBs). Although initially negative for known anti-neural autoantibodies, case 7 developed serum acetylcholine receptor antibodies and myasthenia gravis a year later (thymoma was not detected by chest CT). Case 8 had high-titer GAD65 antibodies in the serum (1389 nmol/L, ref.   0.02) and CSF (36.4 nmol/L, ref.   0.02).

Case 7 had notable improvement of attention, awareness, and cognitive processing after treatment with levetiracetam, high dose oral prednisone, and multiple rounds of plasmapheresis but within the next year suffered a subacute decline in mental status and a recurrence of seizures. He had several body CTs and PET scan without evidence of a tumor. Despite multiple immunotherapies, he continued to decline and passed away about 3.5 years after disease onset. No autopsy was performed. Case 8 initially responded to antiepileptic medications, but her GAD65 antibodies persisted during convalescence (serum, 1983 nmol/L), and her seizures became medically refractory despite glucocorticoids and rituximab. Case 9 experienced a near complete resolution of memory impairment after a combination of chemotherapy and immunosuppression.

Molecular Characterization of TRIM9/67-IgG cases

Summary results across all assays are provided in Figure 1.

Tissue-based immunofluorescence (TBIF) in the murine brain

TRIM9/67-IgG cases were less common than anti-Yo (6 vs 91) and similar to anti-Ri (6 vs 7) when comparing relative frequencies over a single year in the Mayo Clinic Neuroimmunology database (N = 98,984 samples tested by tissue-based immunofluorescence TBIF in 2020). Similarly, at Hôpital Neurologique in 2020, only one patient was positive for TRIM9/67-IgG compared to 15 anti-Yo and 7 anti-Ri (N = 16,910 tested on TBIF). All candidate TRIM9/67 cases were identified by rodent brain tissue staining except cases 7 and 8, which were initially identified by PhIP-Seq. Every case but case 8 produced characteristic widespread immunostaining of neuronal somata in the olfactory bulb, cortex, hippocampus, thalamus, and molecular and Purkinje cell layers of the

cerebellum (Figure 2A).[1] In contrast, case 8 CSF produced a GAD65-like immunostaining pattern, consistent with the patient's known GAD65-IgG positivity.

Using CSF from a representative case (case 1), we found that patient IgG colocalized with anti-TRIM9 in all anatomic regions (Figure 2B). In contrast, cerebellar TRIM67 protein expression was nearly undetectable by TBIF, consistent with six-fold lower cerebellar TRIM67 than cerebellar TRIM9 gene expression according to ProteinAtlas.org[13] (Figure 2C).

Detection of TRIM9/67-IgG by HEK293 cell-based overexpression assay

By CBA, CSF and/or sera from all 13 cases were positive for TRIM9/67-IgG (Figure 3A and B). By end-point dilution series, there was no overall difference between anti-TRIM9 and anti-TRIM67 antibody titers (p=0.45, paired Wilcoxon rank test). However, CSF TRIM9-IgG and TRIM67-IgG titers were lower in encephalitis cases than cerebellar syndrome cases (p=0.0317 and p=0.0159 respectively), but there was no difference in serum titers; nor was there a difference in titers between cases of unknown phenotype and cerebellar cases (Figure 3C). TRIM9 and TRIM67 antibody titers were significantly higher in serum than in CSF (p = 0.002 for both TRIM9 and TRIM67) (Figure 3C). Yet, within samples, TRIM9 and TRIM67 antibody titers were well correlated ($r^2 = 0.78$) (Figure 3D).

Detection of TRIM9/67-IgG by immunoblot

Mass spectrometry previously demonstrated that TRIM9 and TRIM67 are present at 95 kDa whereas only TRIM9 is present at 72 kDa.[1] Therefore, we tested whether immunoblot is as sensitive as CBA. Cases 2, 3, and 4 were previously shown to recognize the 95 and 72 kDa bands.[1,2] CSF from newly reported cases 1 and 5 exclusively recognized the 95 and 72 kDa bands while cases 9 and 11 recognized TRIM9/67 and additional bands, suggesting the presence of other anti-neural antibodies. In contrast, cases 7 and 8 both produced a lower band of approximately 60 kDa but no bands at the expected molecular weights (Figure 3E).

Detection and characterization of TRIM9/67-IgG by PhIP-Seq

We evaluated the sensitivity of PhIP-Seq[14,15] for TRIM9/67 antibodies at the protein and peptide level. At the protein level, 11 of 18 and 7 of 18 biospecimens enriched TRIM9 and TRIM67, respectively (Figure 4A). At the peptide level, 17 and 16 of 18 biospecimens enriched at least one TRIM9 or TRIM67 peptide, respectively (Figure 4A). The dominant peptide for both TRIM9 and TRIM67 mapped to the homologous B-box type 2 domain (B-Box 2), a zinc-finger domain of unknown function (Figure 4B). The B-box 2 epitopes are predicted to be conformational (Figure 4C), and cases that enriched the B-box 2 peptide by PhIP-Seq were positive by TRIM9 or TRIM67 B-box 2 domains by CBA (Figures 1 and 4D); but overall, B-box 2 CBA was less sensitive than whole protein CBA. Curiously, despite their homology, TRIM9 and TRIM67 B-box 2 domains exhibited different subcellular localization.

The fact that some cases were immunoreactive to TRIM9 and TRIM67 by CBA but not denaturing immunoblot suggests that some TRIM9/67 autoantibodies bind to conformational epitopes. However, B-box 2 expression levels were too low to test for

loss of autoantibody binding following denaturing SDS-PAGE. Therefore, we assessed for conformational epitope-dependent TRIM9/67 autoantibodies by immunoprecipitation. We immunoprecipitated mouse brain tissue lysate with CSF from case 8, which failed to enrich or bind to TRIM9 by PhIP-Seq and immunoblot, respectively. Like cases 1 and 7 that did enrich TRIM9 by PhIP-Seq, case 8 immunoprecipitated the three major TRIM9 isoforms (Figure 4E). Likewise, case 7 robustly immunoprecipitated TRIM9 and TRIM67 as determined by IP-MS despite not enriching TRIM67 by PhIP-Seq (Figure 4F).

To further characterize the autoantibody profile of TRIM9/67 syndromes, we expanded our PhIP-Seq analysis to the entire human proteome. To be conservative, we used a previously described analytic approach that looks for sets of overlapping peptides enriched at least 10-fold above controls whereby at least one peptide in the set is enriched at least 100-fold.[10,16] We then compared these candidates to a database of 4,206 healthy serum, healthy CSF, and negative control (bead only) PhIP-Seq runs.

We found that case 9, who had encephalitis and SCLC, enriched ZIC1, a paraneoplastic autoantigen associated with SCLC and paraneoplastic cerebellar degeneration.[17] Previously classified autoantigens were not enriched by other cases. However, case 5 enriched peptides mapping to the B-box type 1 domain of TRIM1 (also known as MID2) and TRIM9 suggesting that anti-TRIM9/67 autoantibodies may cross react with other TRIM family proteins.

We next considered whether TRIM9/67 antibodies might be incidental to a distinct encephalitis syndrome. However, we failed to find a shared alternate candidate autoantigen among encephalitis cases by PhIP-Seq. Nonetheless, we identified candidate autoantigens with putative relevance including SIPA1L1, which may regulate seizure threshold[18] (case 8), and astrocyte-enriched PHF21B, which has been implicated in small cell lung cancer[19] (case 9). Case 7 also enriched peptides to RTP5, an uncharacterized protein that is highly expressed in the hypothalamus[13].

Immunohistochemistry of TRIM9 and TRIM67 in the human brain

Anatomic characterization of TRIM9 and TRIM67 protein expression in the human brain is limited[6,20]. We found human cerebellar TRIM9 expression largely mirrored expression in the murine cerebellum and was characterized by strong immunoreactivity of Purkinje cell bodies, primary and secondary Purkinje cell dendrites, and light staining of the molecular layer neuropil. In contrast, TRIM67 immunostaining was scarcely detected in Purkinje cells, whereas strong nuclear immunoreactivity was observed in granule cells and interneurons in the molecular layer (Figure 5). In human temporal lobe, subtle differences between TRIM9 and TRIM67 protein expression were appreciated. TRIM9 staining was stronger in the outer layers of the temporal lobe relative to deeper layers. In general, in both the entorhinal cortex and hippocampus, the regional expression of TRIM9 and TRIM67 was generally complementary (the inverse of each other) and did not overlap (Figure 5).

TRIM9/67 protein expression in patient cancer

We performed IHC on benign tissue, primary melanoma, and metastatic melanoma from case 1. TRIM9 colocalized with metastatic but not primary melanocytic cells or benign

cells. In contrast, TRIM67 did not preferentially colocalize with either primary or metastatic melanoma cells (Figure 6A – C).

We assessed tumors from four additional TRIM9/67-IgG patients (cases 2–5). Biopsies from cases 2–4 expressed the tumor marker pan-cytokeratin (panCK). Similar to case 1, metastatic SCLC tissue from case 2 had significantly higher anti-TRIM9 immunofluorescence in panCK^{high} than panCK^{low} regions. In contrast, TRIM67 immunofluorescence did not differ between panCK^{high} and panCK^{low} regions. In primary and metastatic lung adenocarcinoma from case 3, both TRIM9 and TRIM67 immunofluorescence were significantly higher in panCK^{high} than panCK^{low} regions. Finally, in primary lung adenocarcinoma from case 4, the relationship between TRIM9 and TRIM67 and panCK varied by cytoarchitecture. TRIM9 and TRIM67 signals were significantly higher in disorganized clusters of panCK^{high} cells, but unchanged in regions where panCK^{high} cells were organized in epithelial or glandular-like arrangements (Figure 6D and 6E). In case 5's ER+ primary and metastatic breast cancer biopsies, we detected qualitatively similar TRIM9 protein expression in ER+ and ER- regions. In contrast to TRIM9, TRIM67 expression was qualitatively lower in ER- regions than ER+ regions (Figure 7).

Discussion

Anti-Yo, -DNER, -KLHL11, and -Ri are well characterized autoantibody biomarkers of paraneoplastic cerebellar degeneration (PCD). However, over two thirds of known paraneoplastic autoantibodies with frequent (>50%) cerebellar involvement are poorly characterized owing to small case numbers, including TRIM9/67-IgG[21]. Here, we performed an extensive search for additional TRIM9/67-IgG cases and confirmed their rarity relative to anti-Yo and anti-Ri antibodies. These additional cases have allowed us to characterize this rare disease more extensively.

Importantly, this expanded TRIM9/67-IgG cohort allowed us to determine that whole protein CBA appears to be the most sensitive TRIM9/67-IgG detection method, with TRIM9 and TRIM67 CBAs being equally sensitive. Of our 13 cases, 10 had available clinical history, and seven of these had cancer, including the second reported case of TRIM9/67-IgG cerebellar syndrome following checkpoint inhibitor therapy (case 1). In addition, case 5 had breast cancer, a new TRIM9/67-IgG cancer association. This expanded cohort indicates that TRIM9/67-IgG are likely high-risk, albeit rare, paraneoplastic autoantibodies that should be included in routine paraneoplastic autoantibody testing.[22] More conservatively, if those cases without available clinical information did not have cancer the TRIM9/67-IgG cancer association drops to 54%, which would place TRIM9/67-IgG in the category of intermediate risk paraneoplastic biomarkers.

This study has revealed that TRIM9/67-IgG cerebellar syndrome is similar to well-characterized PCD associated with intracellular onconeural antigens in many respects. Like anti-Yo[23] and anti-Ri[24], our TRIM9/67-IgG cerebellar cases uniformly had a mild pleocytosis with elevated protein and generally had normal or nondiagnostic MRI findings. Like anti-Yo and anti-Ri, most cerebellar cases had poor outcomes characterized by static

or progressive symptoms. In no case did immunotherapy reverse or improve cerebellar symptoms. However, in contrast to anti-Yo and anti-Ri, melanoma was associated with 29% of known TRIM9/67-IgG patients with cancer (one of whom was on an immune checkpoint inhibitor) and 14% of all TRIM9/67-IgG cases. Melanoma-associated paraneoplastic cerebellar syndromes are exceedingly rare, many of which have been reported without an identified autoantibody[25–30]. Seropositive melanoma-associated paraneoplastic cerebellar cases include SEPTIN3[31] (N = 2), Yo[32] (N = 1), GABABR[33] (N = 1), CARP-VIII[34] (N = 1), ARHGAP26[35] (N = 1), and an anti-TRIM9/67-IgG case (N = 1)[3].

This study highlights some additional benefits of complementing traditional autoantibody discovery and validation methods with PhIP-Seq. As demonstrated here, PhIP-Seq epitope mapping aids direct comparison of paraneoplastic polyclonal antibody responses to paralogous gene pairs like TRIM9/TRIM67; as was also done for CDR2L/CDR2 in anti-Yo paraneoplastic cerebellar degeneration[4,36]. PhIP-Seq may be particularly well-suited to identify autoantibodies elicited by cancer-associated neoantigens, even against a background of systemic autoimmunity[37]. As a massively parallel antibody detection method, PhIP-Seq may also aid in identifying autoimmune neurological patients who harbor additional antibodies that may contribute to illness presentation[38]. Moreover, PhIP-Seq has detected autoantibodies that fail to bind rodent brain tissue[36] or novel autoantibodies that do not recognize a rodent ortholog[39], or for which a rodent ortholog does not exist[40]. However, the sensitivity of PhIP-Seq is hampered by the absence of post-translational modifications and limited conformational representation.

Although PhIP-Seq identified the homologous TRIM9/TRIM67 B-box 2 domains as immunodominant peptide epitopes, not all cases were immunoreactive to this epitope. That some cases recognize TRIM9/67 by IP-MS and CBA but not PhIP-Seq or immunoblot indicates the presence of conformational epitope-dependent TRIM9 and TRIM67 autoantibodies and likely explains the superior sensitivity of CBA, which should inform future diagnostic test design. CBA is also a specific test for TRIM9/67-IgG neurologic autoimmunity. We previously demonstrated that TRIM9/67-IgG was not detected in sera of SCLC patients with a paraneoplastic syndrome (N = 63), sera from lung adenocarcinoma patients with PNS (N = 36), CSF from patients with autoimmune encephalitis (N = 100), or CSF from neurodegenerative disease patients (N = 165)[1]. Furthermore, we did not detect enrichment of TRIM9/67 by healthy CSF (N = 42) or neuroinflammatory CSF with and without cancer (N = 789) in our PhIP-Seq database. Taken together, these data indicate that TRIM9/67-IgG is a specific marker of neurological autoimmunity, most commonly a paraneoplastic cerebellar syndrome. Notably, TRIM46, another class I TRIM family autoantigen, is also a specific marker of diverse autoimmune neurological presentations[41].

Although subacute cerebellar syndrome was the dominant TRIM9/67-IgG phenotype, TRIM9/67 antibody positive encephalitis cases were observed as well. Case 8's presentation was compatible with GAD65 encephalitis. Of note, case 9 enriched ZIC1, a paraneoplastic cerebellar degeneration biomarker[17] by PhIP-Seq. Additionally, we did not detect other classified encephalitis autoantibodies in cases 7 or 9, and both enriched other neural candidate antigens by PhIP-Seq suggesting that their phenotype may have been driven by

another autoantigen. TRIM9-IgG and TRIM67-IgG antibody titers were significantly lower in the CSF and nominally lower is in the serum of TRIM9/67-IgG encephalitis compared to cerebellar cases. Additionally, all tested cerebellar syndrome cases recognized TRIM9/67 by immunoblot, whereas encephalitis cases 7, 8, and 9 and unknown phenotype case 11 recognized bands other than TRIM9/67. Although, extracerebellar features have been observed in other paraneoplastic PCDs, these data suggest that in some cases TRIM9/67-IgG may co-occur in other autoimmune neurological disorders. Nonetheless, because TRIM9/67-IgG is a sensitive and specific marker of neurological autoimmunity, testing may be warranted in seronegative autoimmune encephalitis.

Because both TRIM9[42,43] and TRIM67[44] have been implicated in proliferation and migration of tumor cells, it isn't obvious *a priori* which might be the primary antigen in paraneoplastic cases. The apparent obligate co-occurrence of TRIM9 and TRIM67 autoantibodies is likely due to antibody cross-reactivity mediated by sequence and structural homology. However, while all cases were positive for both TRIM9 and TRIM67 autoantibodies by CBA, patient IgG colocalized with TRIM9 and not TRIM67 in mouse brain tissue. Nonetheless, TRIM67 has been proposed as the primary antigenic target[3] with epitope spreading[45] to TRIM9, but this has not been experimentally confirmed. Here we found higher TRIM9 protein expression in cancer versus noncancer cells in cancer biopsies (n=4/5 cases), and documented TRIM9 and TRIM67 protein expression in a fifth case with primary breast cancer. In contrast, TRIM67 protein was highly expressed in cancer biopsies from only two of the same five patients. These data suggest that in some cases TRIM9 is the antigenic initiator of TRIM9/67 paraneoplastic autoimmunity.

Overall, these studies indicate that TRIM9/67-IgG are high-risk paraneoplastic biomarkers for which CBA is likely the most sensitive assay. Although TRIM9/67-IgG cases were less common than anti-Yo and anti-Ri at two testing sites, systematic testing is required to establish its true prevalence. Future studies of the pathobiology of TRIM9/67-IgG syndromes should include HLA typing with T-cell stimulation assays, comparative genomics of tumors from TRIM9/67-IgG positive and negative patients,[46] and neuropathological characterizations.

Limitations

Of cases with evidence of TRIM9/67 autoimmunity by two methods, CBA was estimated to be 100% sensitive. However, this may be an overestimate due to the limited number of TRIM9/67 cases in this study. Although we report a new association between TRIM9/67-IgG and encephalitis, additional cases are required to determine whether TRIM9/67-IgG is a bystander in autoimmune encephalitis. Our commercial TRIM9 antibody demonstrated cross-reactivity with TRIM67 by CBA but did not overlap with TRIM67 immunostaining in tissue. Nonetheless, we cannot entirely exclude that some tissue TRIM9 signal is due to TRIM67 cross reactivity. Furthermore, while our commercial TRIM67 antibody did not recognize TRIM9, we cannot rule out that it binds to other off-target proteins. PhIP-Seq indicated a more diverse antibody response to TRIM9 than TRIM67 across the cohort. However, the difference in diversity may be due to inherent biases in the composition of the

phage library. Finally, our human brain TRIM9 and TRIM67 staining was limited to a single donor, therefore these findings may not generalize.

Supplementary Material

Refer to Web version on PubMed Central for supplementary material.

Acknowledgements

Data Availability

Raw data were generated at University of California San Francisco and Universités de Lyon. Derived data supporting the findings of this study are available from the corresponding authors on request.

References

1. Do LD, Gupton SL, Tanji K, et al. TRIM9 and TRIM67 Are New Targets in Paraneoplastic Cerebellar Degeneration. Cerebellum Apr 2019;18(2):245–254. doi:10.1007/s12311-018-0987-5 [PubMed: 30350014]

2. Sebbag E, Psimaras D, Baloglu S, et al. Immune-Related Cerebellar Ataxia: A Rare Adverse Effect of Checkpoint Inhibitor Therapy. J Neuroimmune Pharmacol Oct 22 2021;doi:10.1007/s11481-021-10026-3

3. Larman HB, Zhao Z, Laserson U, et al. Autoantigen discovery with a synthetic human peptidome. Nat Biotechnol May 22 2011;29(6):535–41. doi:10.1038/nbt.1856 [PubMed: 21602805]

4. O'Donovan B, Mandel-Brehm C, Vazquez SE, et al. High-resolution epitope mapping of anti-Hu and anti-Yo autoimmunity by programmable phage display. Brain Commun 2020;2(2):fcaa059. doi:10.1093/braincomms/fcaa059 [PubMed: 32954318]

5. Short KM, Cox TC. Subclassification of the RBCC/TRIM superfamily reveals a novel motif necessary for microtubule binding. J Biol Chem Mar 31 2006;281(13):8970–80. doi:10.1074/jbc.M512755200 [PubMed: 16434393]

6. Tanji K, Kamitani T, Mori F, Kakita A, Takahashi H, Wakabayashi K. TRIM9, a novel brain-specific E3 ubiquitin ligase, is repressed in the brain of Parkinson's disease and dementia with Lewy bodies. Neurobiol Dis May 2010;38(2):210–8. doi:10.1016/j.nbd.2010.01.007 [PubMed: 20085810]

7. Winkle CC, McClain LM, Valtschanoff JG, Park CS, Maglione C, Gupton SL. A novel Netrin-1-sensitive mechanism promotes local SNARE-mediated exocytosis during axon branching. J Cell Biol Apr 28 2014;205(2):217–32. doi:10.1083/jcb.201311003 [PubMed: 24778312]

8. Kozareva V, Martin C, Osorno T, et al. A transcriptomic atlas of mouse cerebellar cortex comprehensively defines cell types. Nature Oct 2021;598(7879):214–219. doi:10.1038/s41586-021-03220-z [PubMed: 34616064]

9. Boyer NP, Monkiewicz C, Menon S, Moy SS, Gupton SL. Mammalian TRIM67 Functions in Brain Development and Behavior. eNeuro May-Jun 2018;5(3)doi:10.1523/eneuro.0186-18.2018

10. Song E, Bartley CM, Chow RD, et al. Divergent and self-reactive immune responses in the CNS of COVID-19 patients with neurological symptoms. Cell Rep Med May 18 2021;2(5):100288. doi:10.1016/j.xcrm.2021.100288 [PubMed: 33969321]

11. Zekeridou A, Kryzer T, Guo Y, et al. Phosphodiesterase 10A IgG: A novel biomarker of paraneoplastic neurologic autoimmunity. Neurology Aug 20 2019;93(8):e815–e822. doi:10.1212/wnl.0000000000007971 [PubMed: 31315972]

12. Graus F, Titulaer MJ, Balu R, et al. A clinical approach to diagnosis of autoimmune encephalitis. Lancet Neurol Apr 2016;15(4):391–404. doi:10.1016/s1474-4422(15)00401-9 [PubMed: 26906964]

13. Sjöstedt E, Zhong W, Fagerberg L, et al. An atlas of the protein-coding genes in the human, pig, and mouse brain. Science Mar 6 2020;367(6482)doi:10.1126/science.aay5947

14. Deutscher S Phage Display to Detect and Identify Autoantibodies in Disease. N Engl J Med Jul 4 2019;381(1):89–91. doi:10.1056/NEJMcibr1903249 [PubMed: 31269373]

15. O'Donovan B, Mandel-Brehm C, Vazquez SE, et al. High-resolution epitope mapping of anti-Hu and anti-Yo autoimmunity by programmable phage display. Brain Communications 2020;2(2)doi:10.1093/braincomms/fcaa059

16. Bartley CM, Johns C, Ngo TT, et al. Anti-SARS-CoV-2 and Autoantibody Profiles in the Cerebrospinal Fluid of 3 Teenaged Patients With COVID-19 and Subacute Neuropsychiatric Symptoms. JAMA Neurol Dec 1 2021;78(12):1503–1509. doi:10.1001/jamaneurol.2021.3821 [PubMed: 34694339]

17. Sabater L, Bataller L, Suárez-Calvet M, Saiz A, Dalmau J, Graus F. ZIC antibodies in paraneoplastic cerebellar degeneration and small cell lung cancer. J Neuroimmunol 2008;201–202:163–165. doi:10.1016/j.jneuroim.2008.01.018

18. Matsuura K, Kobayashi S, Konno K, et al. SIPA1L1/SPAR1 Interacts with the Neurabin Family of Proteins and is Involved in GPCR Signaling. The Journal of Neuroscience 2022;42(12):2448–2473. doi:10.1523/jneurosci.0569-21.2022 [PubMed: 35121636]

19. Li C, Zhang J, Yang X, et al. hsa_circ_0003222 accelerates stemness and progression of non-small cell lung cancer by sponging miR-527. Cell Death Dis Aug 25 2021;12(9):807. doi:10.1038/s41419-021-04095-8 [PubMed: 34433810]

20. Yaguchi H, Okumura F, Takahashi H, et al. TRIM67 protein negatively regulates Ras activity through degradation of 80K-H and induces neuritogenesis. J Biol Chem Apr 6 2012;287(15):12050–9. doi:10.1074/jbc.M111.307678 [PubMed: 22337885]

21. Muñiz-Castrillo S, Vogrig A, Ciano-Petersen NL, Villagrán-García M, Joubert B, Honnorat J. Novelties in Autoimmune and Paraneoplastic Cerebellar Ataxias: Twenty Years of Progresses. The Cerebellum 2022/08/01 2022;21(4):573–591. doi:10.1007/s12311-021-01363-3 [PubMed: 35020135]

22. Graus F, Vogrig A, Muñiz-Castrillo S, et al. Updated Diagnostic Criteria for Paraneoplastic Neurologic Syndromes. Neurol Neuroimmunol Neuroinflamm Jul 2021;8(4)doi:10.1212/nxi.0000000000001014

23. Venkatraman A, Opal P. Paraneoplastic cerebellar degeneration with anti-Yo antibodies - a review. Ann Clin Transl Neurol Aug 2016;3(8):655–63. doi:10.1002/acn3.328 [PubMed: 27606347]

24. Luque FA, Furneaux HM, Ferziger R, et al. Anti-Ri: an antibody associated with paraneoplastic opsoclonus and breast cancer. Ann Neurol Mar 1991;29(3):241–51. doi:10.1002/ana.410290303 [PubMed: 2042940]

25. Berger JR, Mehari E. Paraneoplastic opsoclonus-myoclonus secondary to malignant melanoma. J Neurooncol Jan 1999;41(1):43–5. doi:10.1023/a:1006189210197 [PubMed: 10222421]

26. Jung KY, Youn J, Chung CS. Opsoclonus–myoclonus syndrome in an adult with malignant melanoma. Journal of Neurology 2006/07/01 2006;253(7):942–943. doi:10.1007/s00415-006-0026-1 [PubMed: 16715202]

27. Hauspy J, Nevin A, Harley I, et al. Paraneoplastic syndrome in vaginal melanoma: a case report and review of the literature. Int J Gynecol Cancer Sep-Oct 2007;17(5):1159–63. doi:10.1111/j.1525-1438.2006.00857.x [PubMed: 17309666]

28. Dresco F, Aubin F, Deveza E, Revenco E, Tavernier L, Puzenat E. Paraneoplastic Opsoclonus-Myoclonus Syndrome Preceding a Mucosal Malignant Melanoma. Acta Derm Venereol Mar 1 2019;99(3):337–338. doi:10.2340/00015555-3062 [PubMed: 30281137]

29. Jiménez-Zarazúa O, Vélez-Ramírez LN, Alcocer-León M, et al. Paraneoplastic Cerebellar Degeneration Secondary to BRAF Mutant Melanoma Metastasis from an Occult Primary Cancer. Case Rep Oncol May-Aug 2020;13(2):633–642. doi:10.1159/000507729 [PubMed: 32774248]

30. Mondragón JD, Jiménez-Zarazúa O, Vélez-Ramírez LN, et al. Paraneoplastic opsoclonus-myoclonus syndrome secondary to melanoma metastasis form occult primary cancer. Case Rep Neurol Jan-Apr 2019;11(1):66–79. doi:10.1159/000497034 [PubMed: 31543788]

31. Miske R, Scharf M, Borowski K, et al. Septin-3 autoimmunity in patients with paraneoplastic cerebellar ataxia. Journal of Neuroinflammation 2023/03/30 2023;20(1):88. doi:10.1186/s12974-023-02718-9 [PubMed: 36997937]

32. Valpione S, Zoccarato M, Parrozzani R, et al. Paraneoplastic cerebellar degeneration with anti-Yo antibodies associated with metastatic uveal melanoma. J Neurol Sci Dec 15 2013;335(1–2):210–2. doi:10.1016/j.jns.2013.08.026 [PubMed: 24035275]

33. Jarius S, Steinmeyer F, Knobel A, et al. GABAB receptor antibodies in paraneoplastic cerebellar ataxia. J Neuroimmunol Mar 15 2013;256(1–2):94–6. doi:10.1016/j.jneuroim.2012.12.006 [PubMed: 23332614]

34. Bataller L, Sabater L, Saiz A, Serra C, Claramonte B, Graus F. Carbonic anhydrase-related protein VIII: autoantigen in paraneoplastic cerebellar degeneration. Ann Neurol Oct 2004;56(4):575–9. doi:10.1002/ana.20238 [PubMed: 15389893]

35. Wallwitz U, Brock S, Schunck A, Wildemann B, Jarius S, Hoffmann F. From dizziness to severe ataxia and dysarthria: New cases of anti-Ca/ARHGAP26 autoantibody-associated cerebellar ataxia suggest a broad clinical spectrum. J Neuroimmunol Aug 15 2017;309:77–81. doi:10.1016/j.jneuroim.2017.05.011 [PubMed: 28601293]

36. Bartley CM, Parikshak NN, Ngo TT, et al. Case Report: A False Negative Case of Anti-Yo Paraneoplastic Myelopathy. Front Neurol 2021;12:728700. doi:10.3389/fneur.2021.728700 [PubMed: 34744969]

37. Xu GJ, Shah AA, Li MZ, et al. Systematic autoantigen analysis identifies a distinct subtype of scleroderma with coincident cancer. Proc Natl Acad Sci U S A Nov 22 2016;113(47):E7526–e7534. doi:10.1073/pnas.1615990113 [PubMed: 27821747]

38. Martinez-Hernandez E, Guasp M, García-Serra A, et al. Clinical significance of anti-NMDAR concurrent with glial or neuronal surface antibodies. Neurology Jun 2 2020;94(22):e2302–e2310. doi:10.1212/wnl.0000000000009239 [PubMed: 32161029]

39. Bartley CM, Ngo TT, Cadwell CR, et al. Dual ankyrinG and subpial autoantibodies in a man with well-controlled HIV infection with steroid-responsive meningoencephalitis: A case report. Front Neurol 2022;13:1102484. doi:10.3389/fneur.2022.1102484 [PubMed: 36756346]

40. Mandel-Brehm C, Benson LA, Tran B, et al. ZSCAN1 Autoantibodies Are Associated with Pediatric Paraneoplastic ROHHAD. Ann Neurol Aug 2022;92(2):279–291. doi:10.1002/ana.26380 [PubMed: 35466441]

41. Valencia-Sanchez C, Knight AM, Hammami MB, et al. Characterisation of TRIM46 autoantibody-associated paraneoplastic neurological syndrome. J Neurol Neurosurg Psychiatry Feb 2022;93(2):196–200. doi:10.1136/jnnp-2021-326656 [PubMed: 34921120]

42. Wang X, Shu Y, Shi H, et al. TRIM9 is up-regulated in human lung cancer and involved in cell proliferation and apoptosis. Int J Clin Exp Med 2016;9(6):10461–10469.

43. Yang F, Liu H, Yu Y, Xu L. TRIM9 overexpression promotes uterine leiomyoma cell proliferation and inhibits cell apoptosis via NF-κB signaling pathway. Life Sciences 2020;257:118101. [PubMed: 32679146]

44. Jiang J, Ren H, Xu Y, et al. TRIM67 Promotes the Proliferation, Migration, and Invasion of Non-Small-Cell Lung Cancer by Positively Regulating the Notch Pathway. J Cancer 2020;11(5):1240–1249. doi:10.7150/jca.38286 [PubMed: 31956370]

45. Powell AM, Black MM. Epitope spreading: protection from pathogens, but propagation of autoimmunity? Clin Exp Dermatol Jul 2001;26(5):427–33. doi:10.1046/j.1365-2230.2001.00852.x [PubMed: 11488833]

46. Small M, Treilleux I, Couillault C, et al. Genetic alterations and tumor immune attack in Yo paraneoplastic cerebellar degeneration. Acta Neuropathologica 2018/04/01 2018;135(4):569–579. doi:10.1007/s00401-017-1802-y [PubMed: 29299667]
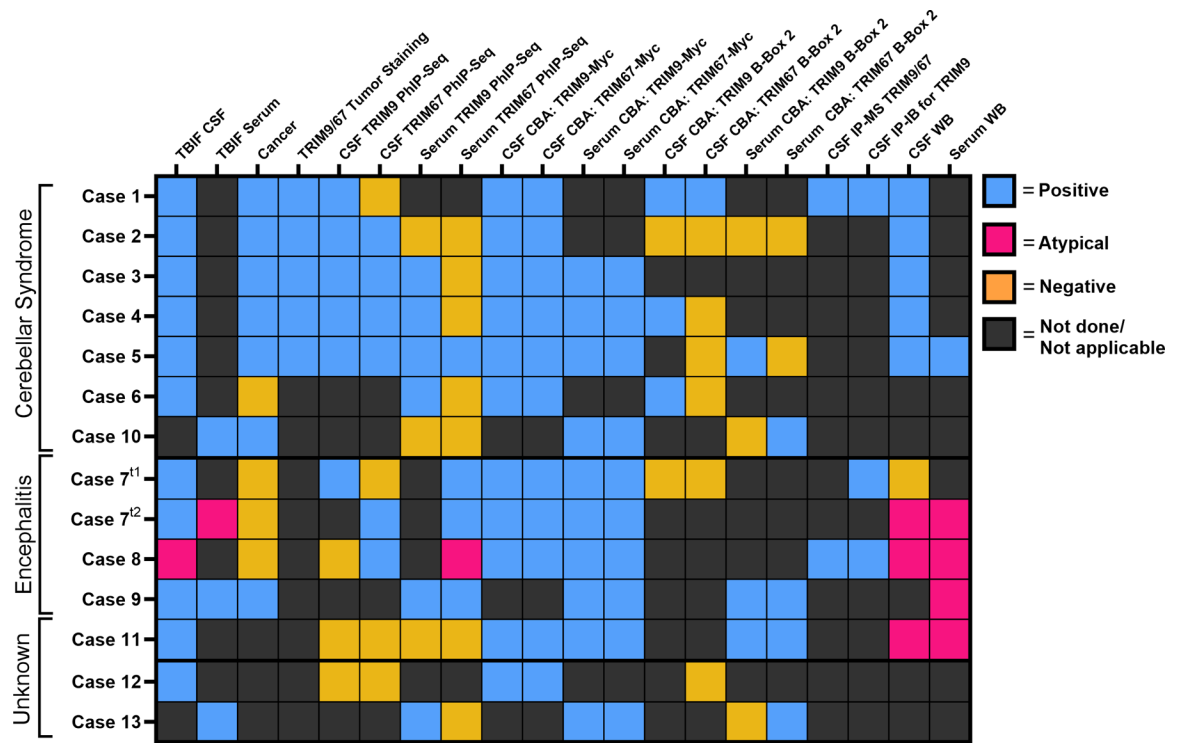
Figure 1.
Cases and biospecimens and outcomes for each assay. Categorical heatmap of cases, assays, and assays results. CBA = cell-based assay, IP-IB = immunoprecipation followed by immunoblot, IP-MS = immunoprecipitation mass spectrometry, PhIP-Seq = phage display immunoprecipitation sequencing, TBIF = tissue-based immunofluorescence, WB = western blot.
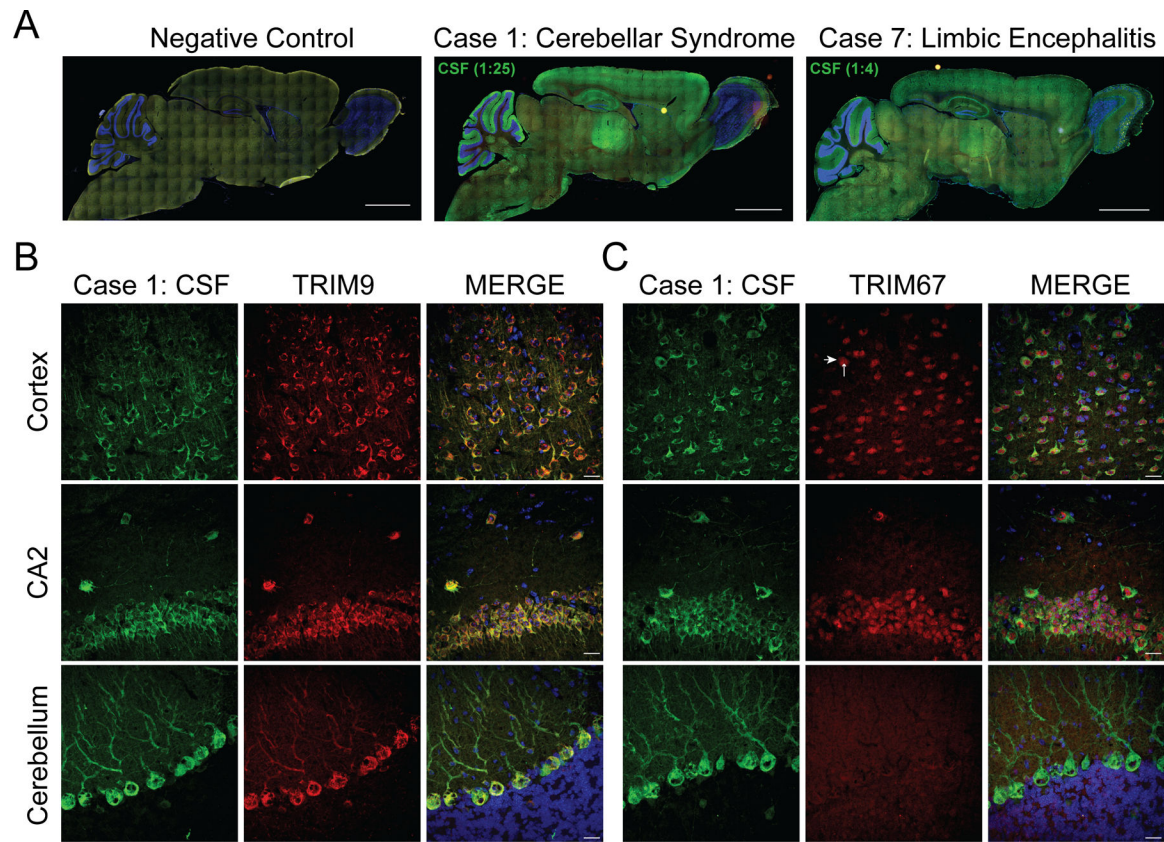
Figure 2.

Tissue-based immunofluorecent assays. A. Panoramic images of CSF IgG (green) from two representative TRIM9/67 cases. Case 1 was immunostained at a 1:25 CSF dilution and case 7 at a 1:4 dilution. Nuclei are stained with DAPI (blue). Scale bars are 2 mm. B. Coimmunostaining of case 1 CSF (green), TRIM9 (red), and nuclei (blue) in the cortex, CA2 of the hippocampus, and cerebellum. Scale bars are 20 μm. C. Coimmunostaining of case 1 CSF (green), TRIM67 (red), and nuclei (blue) in the cortex, CA2 of the hippocampus, and cerebellum wtihout antigen retrieval. Scale bars are 20 μm.
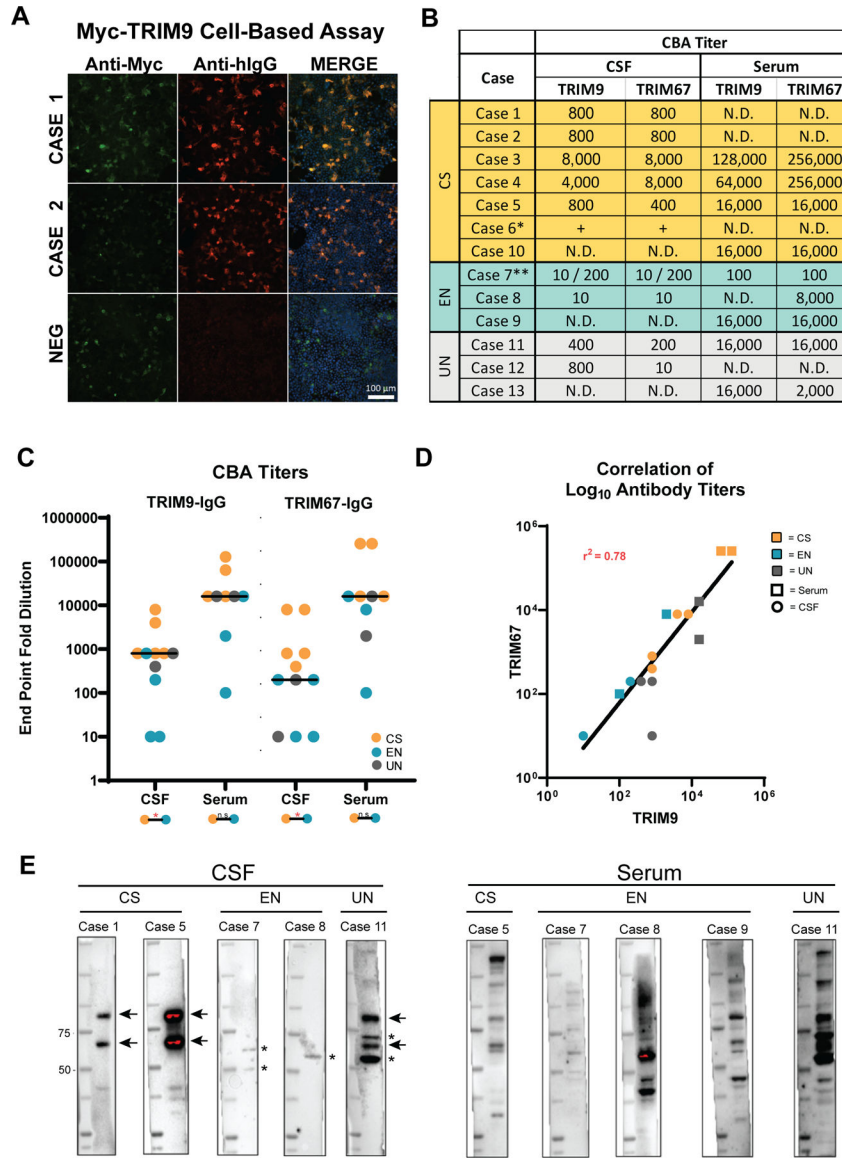
Figure 3.
Validation of TRIM9/67-IgG by CBA and immunoblot. A. HEK 293T cells were transfected with myc-TRIM9 or myc-Trim67 and immunostained with anti-Myc (green), patient CSF or serum (anti-human IgG, red) and DAPI nuclear counterstain (blue). CSF CBAs (1:10 dilution) from two representative cases are shown. Scale bar = 100 μm. B. Table of CBA end point titers. N.D. = not done. * indicates that case 6 was positive by CBA but there was insufficient CSF to complete the dilution series, **indicates that two time points were tested for case 7 CSF (earlier time point to the left of the backslash). CS = cerebellar syndrome, EN = encephalitis, UN = unknown phenotype. C. Dot plots of TRIM9 and TRIM67 autoantibody titers as determined by end point dilution CBAs. Unbroken line = median titer. Barbells below each data column indicate whether there is a significant (*, p < 0.05) or nonsignificant difference between autoimmune encephalitis (EN) and cerebellar syndrome (CS) cases as determined by two-tailed unpaired Mann Whitney tests. UN =

unknown clinical phenotype. D. Log scale scatter plot of within sample TRIM9:TRIM67 autoantibody titer as determined by CBA. r2 was determined by simple linear regression. E. Immunoblots of whole rat brain lysate with CSF and serum. Cases 1 and 5 show the typical banding pattern at 72 kDa and 95 kDa. Cases 7, 8, 9 and 11 show atypical banding patterns as indicated by the asterisks. Black arrows = TRIM9/67 bands. Asterisks = unexpected bands.
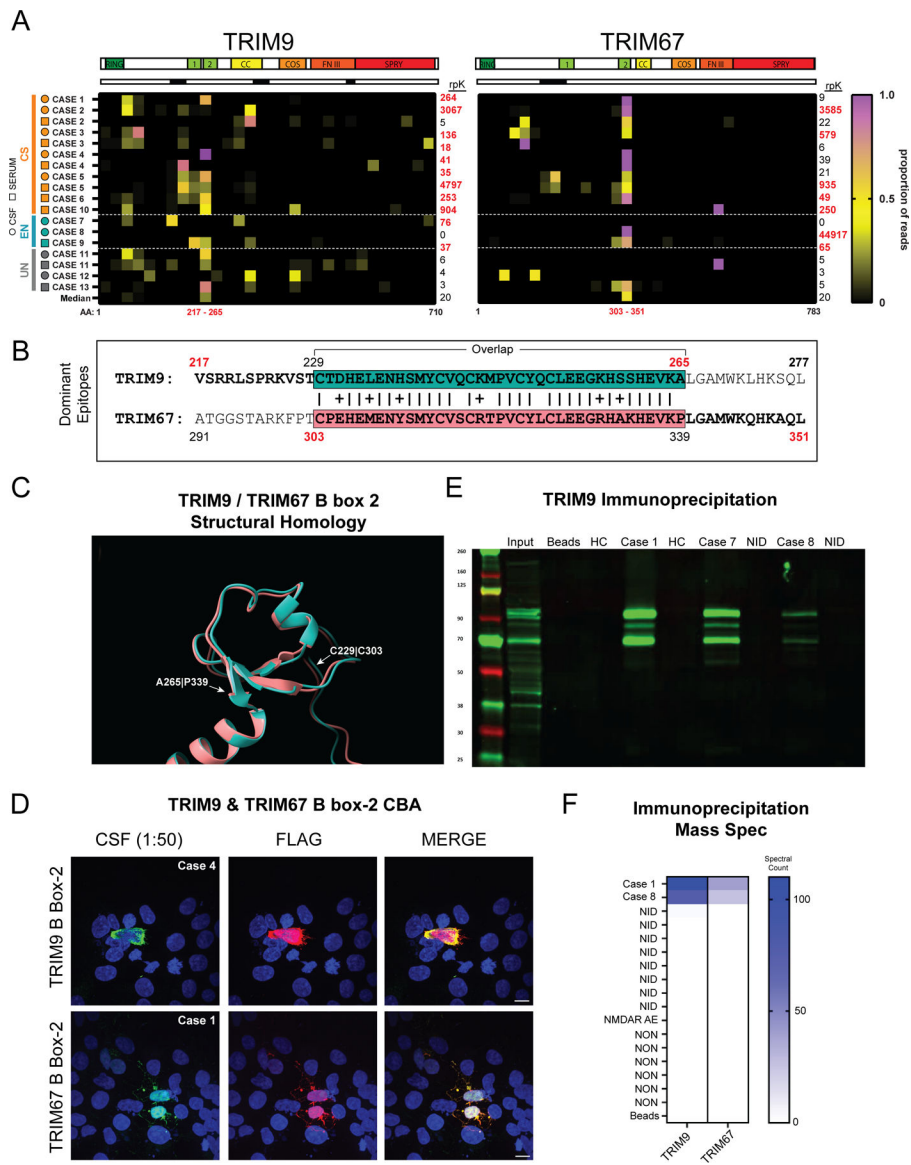
Figure 4.
TRIM9/67-IgG epitope mapping. A. Top, linear TRIM9 and TRIM67 protein structures. Protein domains align to peptides in heatmap below. The white and black band beneath TRIM9 and TRIM67 protein structures denotes peptides (black) enriched by a TRIM9/67-IgG-positive individual from a prior study3. Heatmaps are colored according to the proportion of PhIP-Seq reads that map to individually enriched peptides. Total rpK for TRIM9 and TRIM67 are shown to the left of each heat map; rpK = reads per 100,000, bolded red = rpK significantly greater than controls (Z score   3), black = rpK not significant. CS = cerebellar syndrome, EN = encephalitis, UN = unknown phenotype. The bottom row represents the median enrichment of each peptide across all samples. The red numbers indicate the N and C terminal amino acid (AA) positions for the dominant TRIM9 (Uniprot ID #Q9C026, isoform 1) and dominant TRIM67 (Uniprot ID #Q6ZTA4, isoform 1) peptide. B. Sequences of the dominant TRIM9 and TRIM67 peptides. The bolded

letters between indicated AAs encode target peptides demarcated by red numbers below the heatmap in A. Vertical lines indicate identical AAs in the overlapping region between the dominant TRIM9 and TRIM67 peptide, plus signs indicate chemically similar AAs, and gaps indicate dissimilar AAs. The overlapping sequence is shown in teal (TRIM9) and salmon (TRIM67). C. AlphaFold models were imported into ChimeraX and the B-box 2 domain of TRIM67 (salmon) was aligned to the B-box 2 domain of TRIM9 (teal). D. TRIM9 and TRIM67 B-box 2-FLAG overexpression CBAs. The top row shows case 4 CSF (green) binding to cytoplasmic FLAG-tagged TRIM9 B-box2 (red). The bottom row demonstrates case 1 CSF (green) binding to FLAG-tagged TRIM67 B-box-2 (red). E. Immunofluorescent immunoblot following immunoprecipitation of TRIM9 from mouse brain lysate without CSF (beads) or with CSF from cases 1, 7, 8, healthy controls (HC, N = 2), or other neuroinflammatory cases (NID, N = 2). F. Heatmaps of spectral counts of TRIM9 and TRIM67 peptide identified by mass spectrometry after immunoprecipitation without CSF (beads), or with CSF from cases 1, 8, other neuroinflammatory disorders (NID, N = 8) or noninflammatory CSF samples (N = 6).
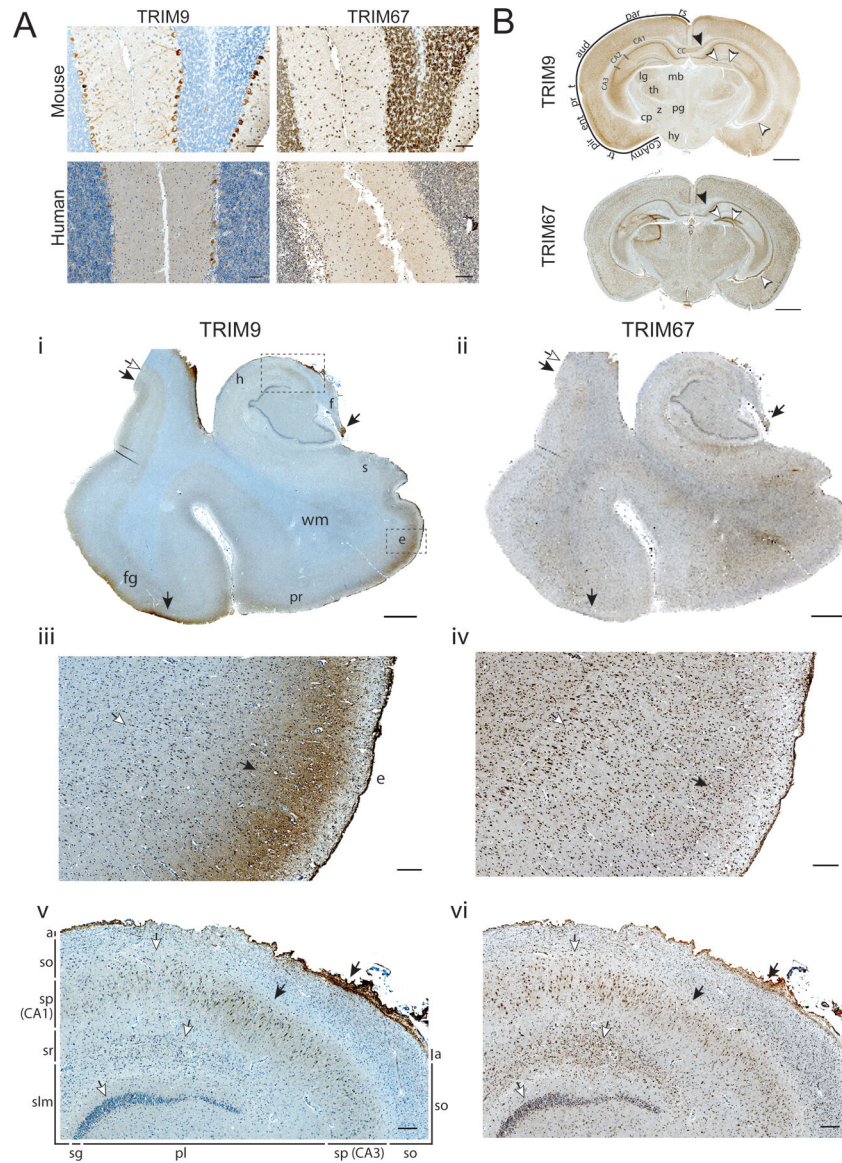
Figure 5.

IHC of TRIM9 and TRIM67 in the murine and human brain (A) 3,3'-diaminobenzidine (DAB) immunostaining of mouse and human FFPE cerebellum. Mouse scale bars = 50 μm. Human scale bars = 100 μm. (B) DAB immunostaining of serial coronal adult mouse brain sections. Anatomic annotations: rs = retrosplenial cortex, par = parietal cortex, aud = auditory cortex, t = temporal cortex, pr = perirhinal cortex, ent = entorhinal cortex, pir = piriform cortex, tr = postpiriform transition cortex, CoAmy = cortical amygdalar layer, cc = corpus callosum, lg = lateral geniculate, th = thalamus, mb = midbrain, z = zona incerta, pg = periaqueductal grey, cp = cerebral peduncle, and hy = hypothalamus. Scale bars = 1mm. (C) i and ii) IHC of serial coronal sections of human medial temporal lobe. Anatomic annotations: h = hippocampus, s = subiculum, e = entorhinal cortex, pr = perirhinal cortex. Upper dashed box indicates region shown in subpanels iii and iv. Lower right dashed rectangle indicates region shown in subpanels v and vi. Scale bars = 2mm. iii and iv) IHC

of TRIM9 and TRIM67 in the entorhinal cortex (e). Scale bars = 200 μm. Throughout the figure, black arrows indicate select regions of TRIM9 > TRIM67 immunoreactivity whereby white arrows indicate select regions of TRIM67 > TRIM9 immunoreactivity. v and vi) IHC of TRIM9 and TRIM67 in serial sections of the human hippocampal formation. Anatomic annotations: a = alveus, so = stratum oriens, sp = stratum pyramidale, sr = stratum radiatum, slm = stratum lacunosum moleculare, sg = stratum granulare, pl = polyform layer/hilus. Scale bares = 250 μm.
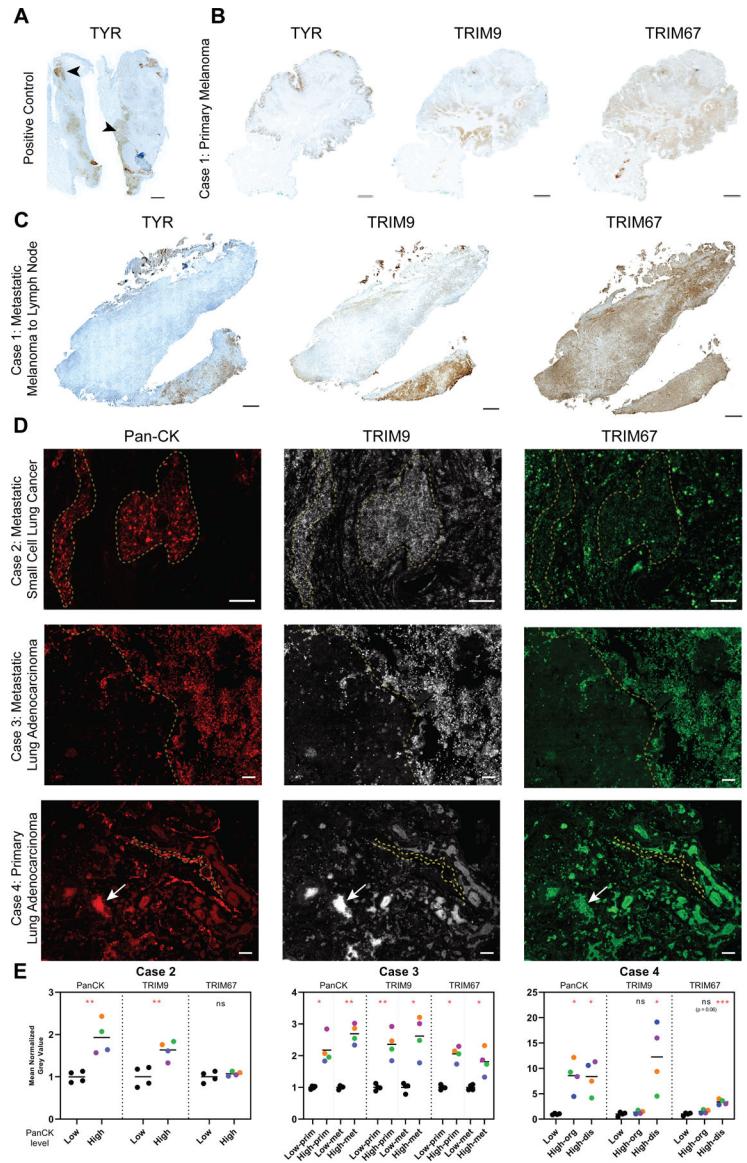
Figure 6.

IHC of TRIM9 and TRIM67 in patient tumors. A. DAB immunostaining of tyrosinase (TYR) in metastatic melanoma to tonsils as a positive control. Scale bar = 1mm. B. Serial sections of case 1 primary melanoma tissue were DAB immunostained for TYR, TRIM9, and TRIM67. Little overlap is observed. Scale bars = 1mm. C. Serial sections from case 1 of metastatic melanoma to lymph nodes were DAB immunostained for TYR, TRIM9, and TRIM67. Visually, the intensity of TRIM9 immunostaining is stronger in TYR+ than TYR- regions. In contrast, the intensity of TRIM67 immunostaining is invariant between TYR+ and TYR- regions. Scale bars = 1mm. D. Multiplex immunofluorescent staining with tumor marker pan-CK clone AE1/AE3 (red), anti-TRIM9 (white), and anti-TRIM67 (green). Case 2, top row: panCK+ areas lie within yellow dotted boundaries. Case 3, middle row: the panCK+ area is to the right of the yellow dotted line. Case 4, bottom row: the parallel yellow lines demarcate a panCK+ cells that are not anti-TRIM9 and anti-TRIM67

immunoreactive. The arrow points to a cluster of panCK+ cells that are immunoreactive to anti-TRIM9 and anti-TRIM67. Scale bars = 50 μm. E. Quantification of the panCK, TRIM9, and TRIM67 immunostaining of tumors shown in 2D. For each antibody, the mean grey value of four panCKlow and four panCKhigh regions of interest (ROIs; Orange = ROI 1, green = ROI 2, blue = ROI 3, purple = ROI 4) was measured. Mean grey values were normalized to the mean of the four panCKlow ROIs. For case 3, two tumor tissues were evaluated: primary (prim) and metastatic (met). For case 4, mean grey value measurements from cytoarchitecturally organized (org) and disorganized (dis) ROIs were taken from within the same primary tumor tissue. P-values were calculated using unpaired, two-tailed t-tests with Welch's correction when appropriate. ns = not significant given a significant threshold of 0.05 (ns > 0.05, * 0.05, ** 0.01, *** 0.001)
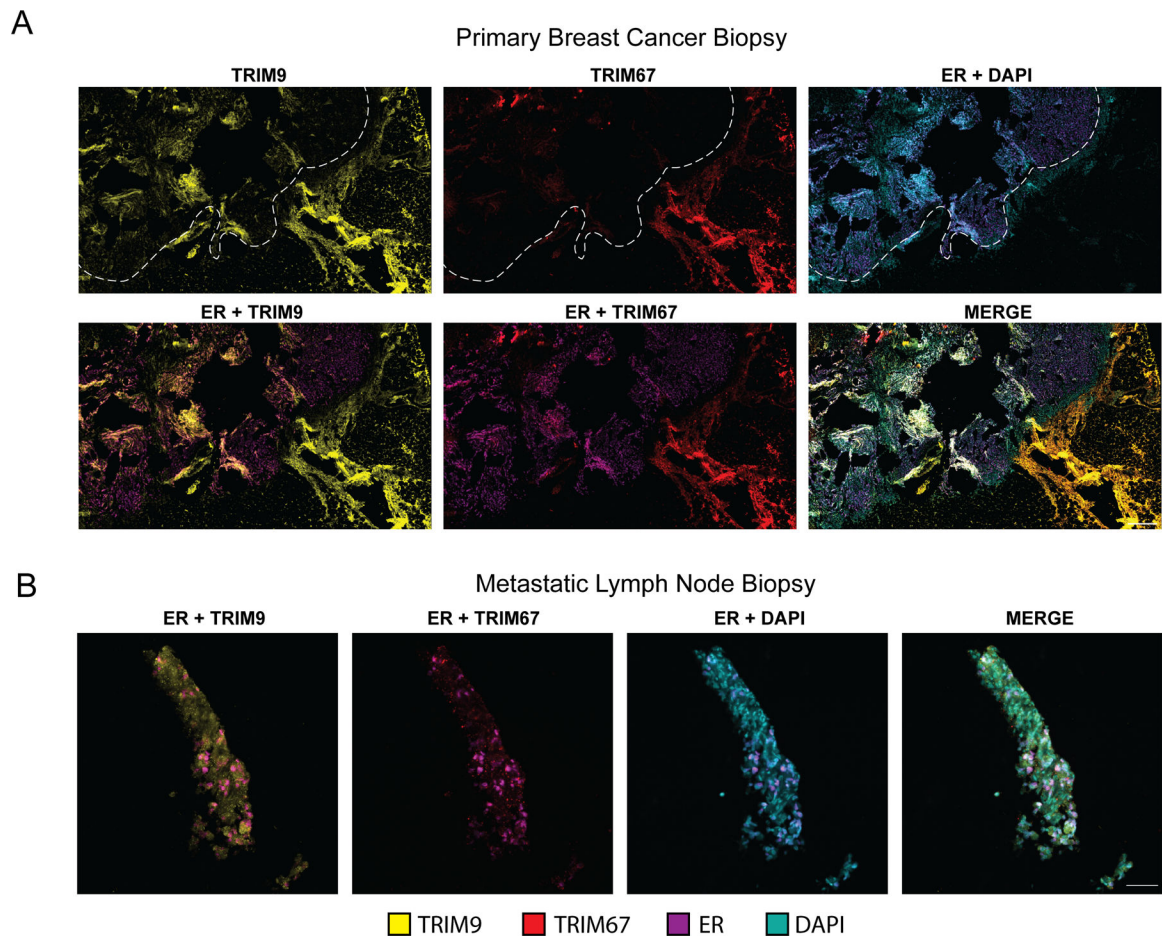
Figure 7.
TRIM9 and TRIM67 protein expression in case 5 breast cancer. A. Multipleplex immunofluorescence (mIF) for TRIM9, TRIM67, ER, and DAPI on primary breast cancer tissue. The dotted line indicates the boundary between ER+ (left) and the ER- (right) region of the tissue. Scale bar = 500μm. B. mIF of metastatic breast cancer to lymph node. Scale bar = 50μm.